

Rapid Prototyping for Aerospace Launch Vehicles

K. Siva Prasad^{*}, E.Rathakrishnan⁺, Sanjay.G .Dhande^{*}

^{*}Department of Mechanical engineering, IIT-Kanpur, India

⁺Department of Aerospace Engineering, IIT-Kanpur, India

Reviewed, accepted August 28, 2003

Abstract

Initial studies of the aerodynamic characteristics of proposed launch vehicles can be made more accurately if lower cost, high-fidelity aerodynamic models are available for wind tunnel testing early in design phase. Rapid Prototyping (RP) is an emerging key technology for producing accurate parts directly from CAD models quickly, with little need of human intervention. Use of RP models was studied at the NASA Marshall Space Flight Center (MSFC). It was concluded that RP methods and materials can be used only for preliminary design studies and limited configurations because of the RP material properties that allow bending of models under higher loading conditions. The reported results and analysis were based on wind tunnel balances. These balances give total load on the body. Thus, there is a need for studying the pressure distribution, the wave pattern and the system behavior under high-speed conditions. In order to study the above goals, a blunt nose cone of a launch vehicle/ missile was tested which was made using the solid based RP method FDM, with a Mach number of 2.0. It is concluded that RP models can take the load at the Mach number 2.0 and also can capture the pressure distribution and wave pattern.

1. Introduction

Since ancient times, making and testing of prototype is a usual practice before going to the final production. Especially in aerospace industry, this is a crucial stage because one can get the aerodynamic characteristics of the proposed launch vehicle. The fabrication of these prototypes is experimented with many forms like material removal process, castings, injection molding etc. Before 1980, the techniques used making of prototypes were craft based and extremely labor intensive. In early 1980's the concept of prototyping had changed slightly called soft or virtual prototyping. The models can be made virtually and these can be stressed, tested, analyzed and modified as if they were physical prototypes. In addition, prototypes tend to become relatively more complex about twice the complexity as before 1980. Correspondingly, the time required to make physical models increased tremendously but the building of physical prototype still depended on craft based methods in spite of the introduction of better precision machines (like CNC machines). In mid 1980's the key prototyping technology called Rapid Prototyping (RP) evolved to speed up the prototype manufacturing process. RP is a term, which embraces a range of new technologies for producing accurate parts directly from CAD models with a little need of human intervention. RP of physical parts is also known as solid free form fabrication (SFF), desktop manufacturing or layer manufacturing technology. Till today, making

functional prototype from RP is one of the challenging tasks. In the present work, an attempt is made to make a functional prototype called wind tunnel models for aerospace applications. There are two important issues in RP to employ it for making wind tunnel models. They are structural integrity and surface roughness. To improve the structural strength of RP models one has to know the maximum loading distribution on the model. The present work demonstrates the measurement of the pressure distribution on the wind tunnel model so that one can understand the loading distribution on the model.

2. Literature Review

Preliminary aerodynamic assessment of future launch vehicle configurations through RP models was studied by NASA Marshall Space Flight center. It was shown to be feasible in limited direct application to wind-tunnel testing. There will be a tremendous advantage in cost savings, model design time and fabrication time; about factor four compared to standard model design and fabrication process. It was concluded that FDM and SLA produced satisfactory results for low speed conditions and diverging at higher loading conditions because RP material properties allow bending of model components under high loading conditions [1]. To improve bending resistance one has to concentrate on the pressure distribution on the body. The NASA results are based on the strain gauge balance. This balance gives total lift, drag and load on the body. There is no information regarding pressure distribution on the body. In this direction, Siva et. al. [2] made an attempt to find out the pressure distribution on RP circular cylinder at a supersonic speed. They studied pressure distribution both quantitatively and qualitatively. There was no permanent deformation in the shape and the experiments were found to be repeatable 100%. In the similar direction an attempt has been made to find out the pressure distribution over a blunt nose cone body both quantitatively and qualitatively, in the present study.

3. Model Construction

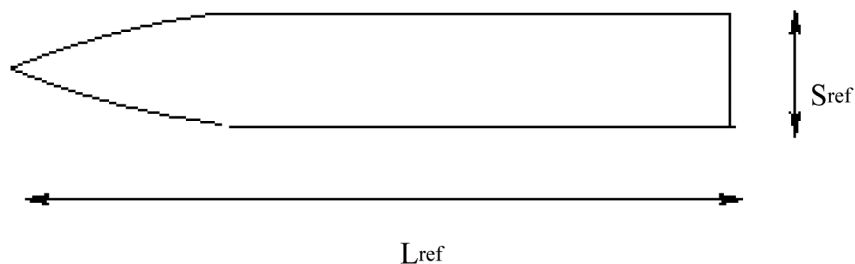


Fig. 1 Geometry of the Blunt Nose Cone Body.

A blunt nose cone body has been chosen for the present study. The model (shown in Fig. 1, $L_{ref} = 60$ mm, $S_{ref} = 314$ mm²) is made out of a solid based RP method FDM (Fused Deposition Modeling). The 3D model is converted into STL (Stereolithography) format in the CAD systems and sent to the FDM slicing software, called Quick Slice. There the STL file is sliced into thin-cross sections of desired thickness, creating a .SLC file (Slice format file). Supports are created for overhanging parts and sliced as well. The sliced model and support are converted into a .SML file (Stratasys Machine Language) that contains actual instructions for the FDM machine. A tool path is generated which is followed by the numerically controlled extruder head. As the head moves in X and Y- directions following the tool path, the thermoplastic material is extruded out of a nozzle and then deposited in ultra thin layers, one layer at a time. Since the envelope surrounding the head is maintained at a temperature below the melting point of material, the extruded material quickly solidifies [3, 4]. The extruder head has two nozzles, one for the part material and the other for the support material. The support can be easily removed by breaking away. The part is built on a foam foundation attached on a Z-stage platen. The Z-stage platen moves downwards as the part is built progressively.

4. Test Facility

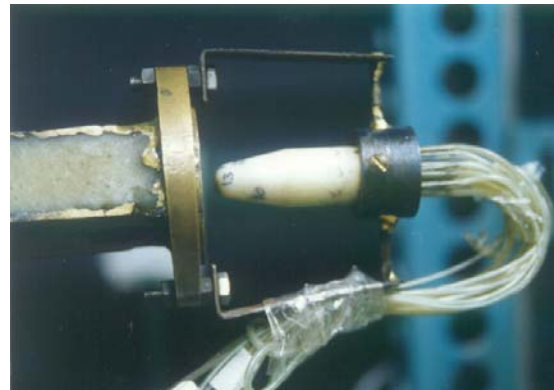


Fig. 2 Open Jet Facility at I.I.T-Kanpur, India Fig. 3. Model Mounted on Wind tunnel

The experiments were conducted in the jet facility at High speed Aerodynamics Laboratory, Indian Institute of Technology Kanpur, India. The test facility consists of compressor, storage tanks and jet test facility as shown in Fig. 2. A two - stage reciprocating compressor capable of delivering 360 cfm of air at a pressure of 500 psi is used in this laboratory. The compressed air is then passed through a pre-filter consisting of porous stone candles to remove solid contaminates, like rust particles and oil droplets. An activated carbon filter is used for finer filtering. The compressed air is dried in a dual tower semi-automatic silica gel driver. While one tower is in use, a portion of the dried air is heated and used to reactivate the other. A diaphragm type back pressure valve operated by pressure relief pilot permits the dryer to operate at 500 psi, while the pressure in the storage tank builds up from atmospheric to storage pressure. The compressed air is stored in three tanks, having a total capacity of 300 ft³ at 300 psi. The pitot pressure sensed by the probe was measured using a PSI model 9010, 16-channel

pressure transducer (interfaced with a PC386). The model 9010 transducer is capable of measuring pressure up to 300 psig, which is approximately 20 atm. The accuracy of the transducer (after rezero calibration) is specified to be $\pm 0.15\%$ full scale.

5. Flow Structure

The kinetic theory says that flow consists of a large number of fluid molecules in unit volume and the transport of mass, momentum and energy takes place through the motion of these molecules. Also, the molecules carry the signals about the presence of the disturbance around the flow field at a speed equal to speed of sound. When the incoming stream is subsonic i.e. the flow speed is less than the speed of sound and the molecules far upstream of the cylinder get the information about the presence of the body through the signals which travel with speed, a_∞ well in advance before reaching the cylinder. Therefore, the molecules orient themselves in order to flow around the cylinder. But when the incoming stream is supersonic, the molecules travel faster than the signals, and there is no possibility that they will be informed of the presence of the body, before they reach the cylinder. Also, the reflected signals from the face of the cylinder tend to coalesce a short distance ahead of the body. Their coalescence forms a thin compression front called shock wave (as shown in Fig. 4).

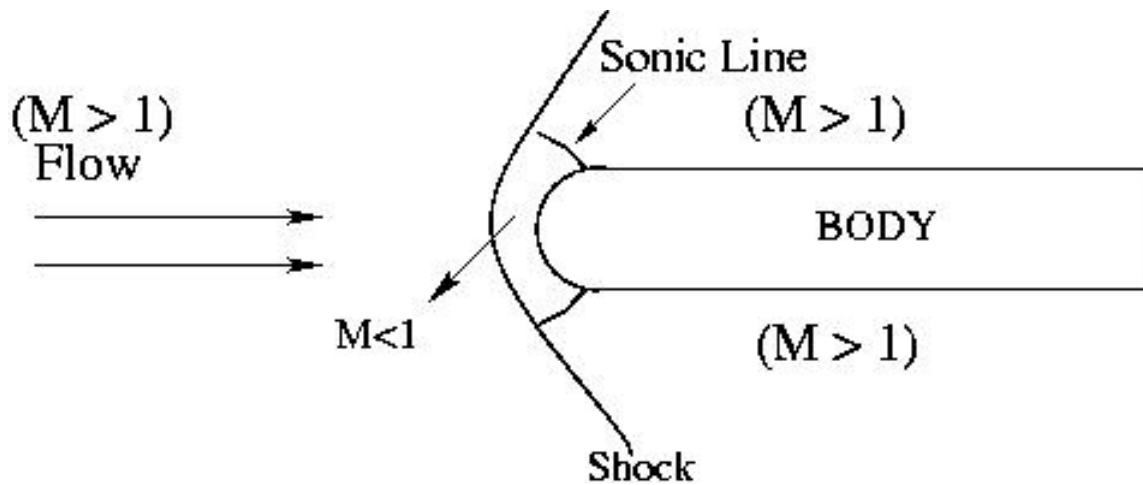


Fig. 4 Physical Significance of the Flow

In the flow process, across the front results in an abrupt change in fluid properties. The thickness of the shock is comparable to the mean free path of the gas molecules in the flow field. The formation of shock takes place after the fluid molecules impinge on the face of the cylinder and rebound. The shock formed normal to the flow direction is called normal shock. The compression wave inclined to at an angle to the flow is called oblique shock. So, the normal shock is a special case of oblique shock. Upstream of the shock, the flow has no information about the presence of the body. However, the streamlines behind the normal shock quickly

compensate for the obstruction, since the flow is subsonic after a normal shock [5]. Oblique shocks usually occur when a flow is turned into itself i.e. when a supersonic flow is turned away from itself, results in the formation of an expansion fan.

The flow is deflected into itself by the oblique shock. All the streamliners are deflected to the same angle at the shock, resulting in an uniform parallel flow downstream of shock. The angle is referred to as flow deflection angle. Across the shock wave, the Mach number decreases and the pressure, density and temperature increase. The corner which turns the flow into itself is called compression or concave corner. In contrast, in an expansion or convex corner, the flow is turned away from itself an expansion fan. All the streamlines are deflected to the same angle after the expansion fan, resulting in uniform parallel flow downstream of the fan. Across the expansion wave, the Mach number increases and the pressure, density and temperature decreases. The flow turns suddenly across the shock and the turning is gradual across the expansion fan, and hence the flow properties through the expansion fan change smoothly, with the exception of the wall streamline where change is sudden. Thus, a model exposed to a supersonic flow experiences a combination of impact, gradual and sudden changes in the loading distribution. Hence, a RP model sustains a supersonic flow can be viewed as appropriate for aerospace application demanding structures with this kind of capability.

6. Results and Discussion

A blunt cone followed by a cylindrical body (stem) is one of the typical shapes of high-speed vehicles like missiles/launchers. Therefore, in the present study, one such typical shape is fabricated out of RP as shown in Fig. 3 and tested at Mach 2.0. This offers a natural advantage to the present investigation which aims at studying RP models behavior under varying aerodynamic loading conditions. The flow field over this body is a complex one, involving detached shock, expansion fan and compression waves. The interaction of these waves causes a considerable impact and shear load. To understand the loading on the blunt nose-cone cylinder combination was tested at Mach 2.0, the model was provided surface pressure taps at $X/D = 0.1, 0.25, 0.5$ and 2.25 at NPRs 4 to 9, insteps of 1. These NPRs (Nozzle Pressure Ratio) were chosen in such a manner that the Mach 2.0 flow is coming with overexpanded state with adverse pressure gradient at NPR 4, 5, 6, nearly correctly expanded state at NPR7 and underexpanded state with favorable pressure gradient prevails at NPR 8, 9. The model will be experiencing all the three kinds of above expansion. Further, the nature of waves will be strongly influenced by the level of expansion. To investigate the behavior of RP model under the said complex situation was studied both qualitatively and quantitatively. The surface pressures were measured for quantitative analysis and flow field was visualized for qualitative analysis.

The measured pressures have been made non-dimensional with reference to the flow field downstream of the detached shock standing a head of the blunt nose. It is essential to note that the flow field downstream of bow/detached shock is a complex one since the Mach number in the field varies from subsonic at the centerline to supersonic as we move along the shock direction. Therefore, identifying a free stream reference dynamic pressure for entire flow field is impossible. So, the dynamic pressure along the axial line just downstream of bow shock has been taken as representative dynamic pressure since the flow is subsonic at the zone and hence at the

nose at C_p should be +1. This can be validation of the measured data and calculation procedure. It should be re iterated here that C_p values at other location should be considered as qualitative but they can serve as reasonable estimate of load on model understanding the load acting on the model.

In the present study, two planes chosen along the model from nose to the base. Along axis1 (shown in Fig 5) is seen that C_p at nose is +1, this clearly indicates that the validity of the present measurement, since it agrees exactly with the theory. At an axial location $X/D = 0.25$, the C_p becomes much larger than unity, indicating that the flow is accelerating from $X/D = 0$ to 0.25. This is because the region between the detached shock and nose faces a normal shock at the nose point in line with the axis of the model and oblique shock for the location away from the shock. The oblique shock progressively becomes weaker with increase of transverse distance from the axis. This results in continuous increase of Mach number at downstream of shock in the transverse direction. Due to this the pressures measured at locations away from $X/D = 0.0$ up to $X/D = 0.25$ are experiencing C_p which are considerable higher than one (reference dynamic pressure just downstream location). The C_p goes to close to zero at $X/D = 0.5$ indicating that the flow continuously accelerates downstream of the nose. For $X/D = 2.25$ location which is on the horizontal stem the C_p becomes negative. The NPR dictates the level of expansion at the nozzle exit influences the flow around the model significantly. From $X/D = 0$ to 0.5, the C_p increases at all locations compared to lower NPRs where as from $X/D = 0.5$ to 2.25, the C_p assumes considerable lower values compared to lower NPRs. This is because as the NPR increase, the shock at the nose moves closer to the body and also the curvature of the bow shock decreases. This makes the normal portion of the bow shock stronger and the oblique weaker as NPR increases. Due to this variation of the nature of the shock, the shock strength and the flow field at the downstream of the shock is strongly influenced by the NPR. For the present investigation, this can be regarded as welcome distribution since it is the primary objective here to study the RP model exposed to a supersonic stream which offers a varying pressure load on the model from nose to tail. The result on another axis is shown in Fig. 6. Here again the behavior is similar to axis1 and reveals that X/D is stronger in between 0.25 to 0.5 and is closer to zero and stays up to 0.5. But the pressure load from 0.5 to the end is not influenced by the axial location.

To have an understanding of the waves present around the RP model, the flow field was visualized in fig 7 to 13, for different NPRs. It is interesting to note that the NPR has strong influence on the wave pattern around the model. With increase of NPR, the wave moves closer to the model and also the interaction of the waves around the model is severe. The combined effect of the interaction causes varying pressure load on the model as seen from C_p plots.

7. Conclusions

A blunt nose cone body was tested at Mach 2.0 speed at different NPRs to demonstrate the feasibility of functional testing of RP models for high speed applications. The surface pressures were measured on the body both quantitatively and qualitatively. RP model is experiencing the severe drag due to differential loading on the model. The load patterns indicate that the skin friction action on the surface is considerable. The model has been exposed to the

complex field continuously during the order of tens of minutes for every NPR to ensure that the model does not suffer any surface damage effect due to the aerodynamic load acting at Mach 2.0. A thorough inspection revealed that the model surface was intact free from any surface defect. Therefore, it can be stated that the RP is suitable for model to fly at supersonic speeds.

References

1. A. Springer, "Evaluating Aerodynamic Characteristics of Wind – Tunnel Models Produced by Rapid Prototyping", *Journal of Spacecraft And Rockets*, 1998, Nov – Dec, Vol 35, No. 6, November – December, pp 755 - 759.
2. K. Siva Prasad, E. Rathakrishnan and S. G. Dhande, "Rapid Prototyping for Supersonic Bluff Bodies", *Proceedings of RPSI, An International Symposium*.
3. Kai, Chua Chee and Fai, Leong Kah, 1997, *Rapid prototyping Principles & Applications in Manufacturing*, John Wiley & Sons, N Y, USA.
4. Pham, D. T., and Gault, R. S., 1998, "A Comparison of Rapid Prototyping Technologies", *Int. J. Mach Tools and Manf.* 38, pp. 1257-1287.
5. E. Rathakrishnan, "Gas Dynamics", Prentice – Hall of India Private Limited, New Delhi, 2001.

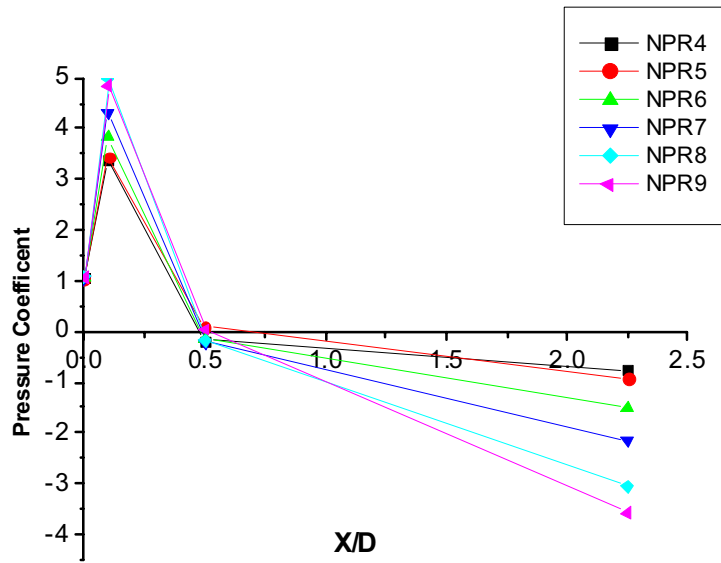


Fig. 5: Pressure Coefficient distribution along the axis 1

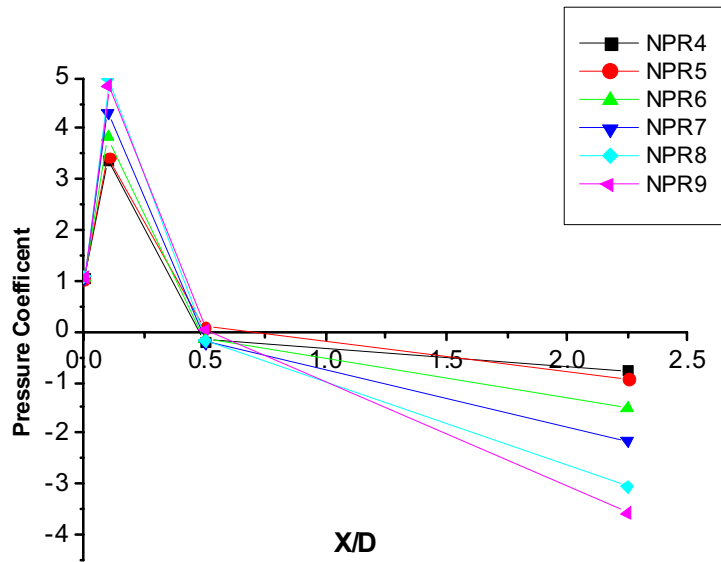


Fig. 6: Pressure Coefficient distribution along the axis 2



Fig. 7 Wave Pattern at NPR 4



Fig. 8 Wave Pattern at NPR 5

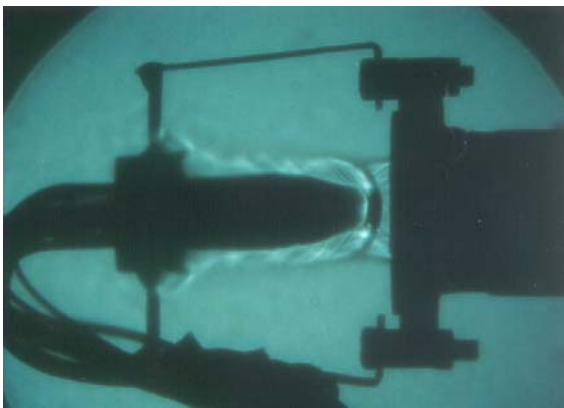


Fig. 9 Wave Pattern at NPR6



Fig. 10 Wave Pattern at NPR7

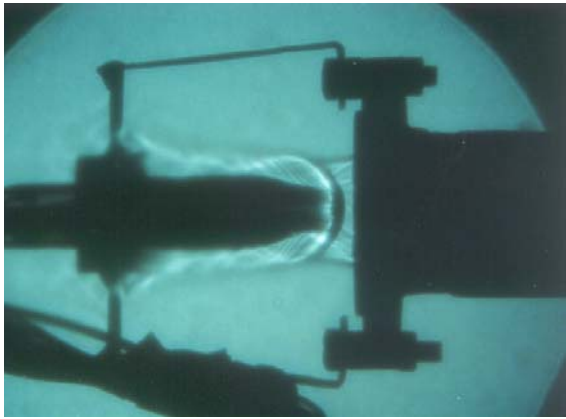


Fig. 11 Wave Pattern at NPR8

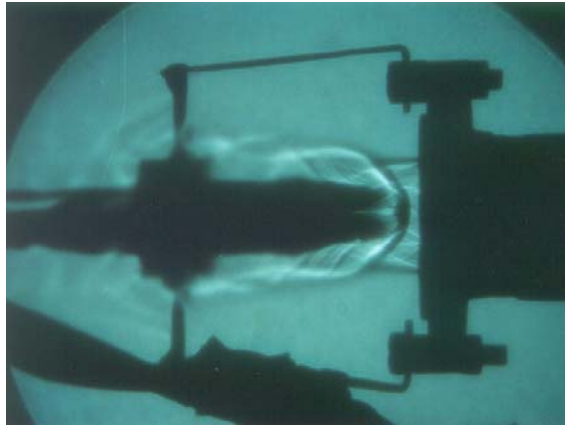


Fig. 12 Wave Pattern at NPR9

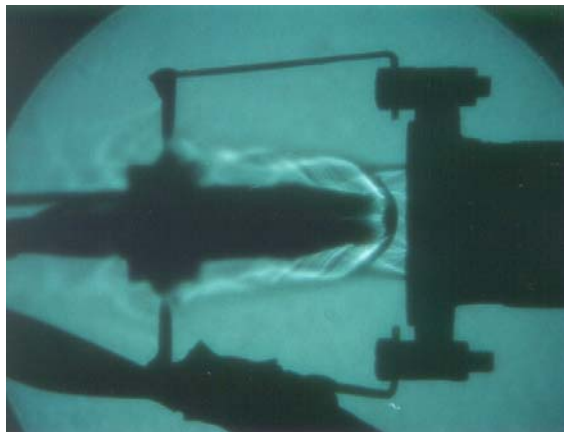


Fig. 13 Wave Pattern at NPR 10